geoconvention
Calgary • Canada • May 15-19 2017

Evaluating the potential of reflection-based waveform inversion

Khalid Almuteri, Kris Innanen and Yu Geng
CREWES – University of Calgary

Summary

Full waveform inversion (FWI) is a powerful tool to build high-resolution velocity models, from recorded seismic data. However, a major issue with FWI is that it fails at reconstructing the low-wavenumber components in the absence of low-frequency information in the data. Generally, for a limited-offset acquisition geometry, deep targets are only sampled by reflected waves with narrow scattering angles, which makes such failure inevitable. In this paper, we point out the limitation of conventional FWI when applied to reflection data, and review an alternative approach to overcome this limitation. The new waveform inversion formalism relies on decomposing the subsurface model into a background part that we seek to resolve, and a reflectivity part that we assume to be known. We show that separating the decoupled velocity model into long-wavelength and short-wavelength components permit us to extract the contribution of the reflected data to the background part of the velocity model.

Introduction

Full waveform inversion (FWI) is an ill-posed data-fitting procedure that aims at reconstructing the earth's physical parameters by iteratively minimizing the least-squares norm of the difference between the predicted and observed data (Lailly, 1983; Tarantola, 1984; Virieux and Operto, 2009). The rise of FWI, as a tool for velocity model building, is due to the high-resolution velocity models that it provides (Pan and Innanen, 2015). The resolution of the FWI reconstruction is related to the diffraction tomography principle (Devaney, 1982; Miller et al., 1987; Wu and Toksöz, 1987; Brossier et al., 2015); which relates the recoverable wavenumber $\boldsymbol{k}$, sampled at a point diffractor (Figure 1), to the local wavelength and aperture angle $\boldsymbol{\theta}$ according to

$$\boldsymbol{k} = \frac{4\pi}{\lambda_0}\cos\left(\frac{\theta}{2}\right)\boldsymbol{n},$$

Where λ_0 is the local wavelength, and $\boldsymbol{n} = \frac{\boldsymbol{q_s}+\boldsymbol{q_r}}{\|\boldsymbol{q_s}+\boldsymbol{q_r}\|}$ (Figure 1).

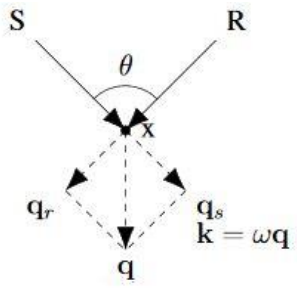

Figure 1: Illustration of the relationship between the wavenumber $\boldsymbol{k}$ and the acquisition geometry for a point diffractor. $\boldsymbol{S}$ denotes source, $\boldsymbol{R}$ denotes receiver, θ is the aperture angle, x is a point diffractor, $\boldsymbol{q_s}$ and $\boldsymbol{q_r}$ are the slowness vectors, $\boldsymbol{q} = \boldsymbol{q_s} + \boldsymbol{q_r}$, ω is the angular frequency, and $\boldsymbol{k}$ is the recoverable wavenumber.

In a narrow-aperture acquisition geometry, where the depth of investigation is larger than the offset range, the shallow area of the subsurface is sampled by reflections, refractions, and direct waves; while

only reflections sample the deep section. According to the diffraction tomography principle, in the deep part of the model, due to the small range of θin narrow-aperture acquisition with smooth background velocity, only high-wavenumbers will be reconstructed, while in the shallow part both low and high wavenumbers will be reconstructed (Brossier et al., 2015); hence, a successful FWI requires the presence of long-offset data, low frequency data, and an accurate starting model.

An alternative approach to the conventional FWI, which aims at retrieving the low-wavenumber components of the velocity in areas sampled by reflected data only, is proposed by Xu et al. (2012), which is known as reflection-based waveform inversion (RWI). In this new approach, the velocity model is decomposed into a background/transmission model that we seek to resolve and a reflectivity model that is assumed to be known, allowing the emphasis on the transmission wavepaths of the reflected data in the inversion process. There are three main differences between conventional FWI and RWI. First, the primary goal of RWI is to invert for the background model, and not to obtain a high-resolution model. Second, FWI uses the full wavefield in the inversion process, including direct waves, refracted and reflected waves, while RWI uses only reflected waves. Third, RWI relies on a migration/demigration process (Zhou et al., 2012).

Method

We start by defining the wave equation in an acoustic medium as

$$[\nabla^2 + \omega^2\mathbf{m}]\mathrm{G}(\mathbf{r}_\mathrm{g}, \mathbf{r}_\mathrm{s}, \omega) = \delta(\mathbf{r} - \mathbf{r}_\mathrm{s}),$$

Where $\mathbf{m} = \mathbf{m}_0 + \delta\mathbf{m}$, is the actual subsurface slowness-squared model, $\mathbf{m}_0$ is the background model, $\delta\mathbf{m}$ is the reflectivity model, $G(\mathbf{r}_\mathrm{g}, \mathbf{r}_s, \omega)$ is the observed data sampled at $\mathbf{r}_\mathrm{g}$ due to a source at $\mathbf{r}_\mathrm{s}$. We define the misfit function as the least-squares norm given by

$$\mathrm{E}(\mathbf{m}_0) = \frac{1}{2}\left\|G(\mathbf{r}_\mathrm{g}, \mathbf{r}_s, \omega) - G_0(\mathbf{r}_\mathrm{g}, \mathbf{r}_s, \omega)\right\|^2 = \frac{1}{2}\left\|\delta\mathrm{P}(\mathbf{r}_\mathrm{g}, \mathbf{r}_s, \omega)\right\|^2$$

Where G_0 is the predicted data and $\delta\mathrm{P}$ is the data residual. In waveform inversion, we aim at minimizing the misfit function, $\mathrm{E}(\mathbf{m}_0)$, by finding an optimum model, $\mathbf{m}$. In conventioal FWI, the gradient, the derivative of the misfit function with respect to the model parameters, or the opposite of update direction is given by

$$\mathrm{g}(\mathbf{r}) = \sum_{\mathbf{r}_\mathrm{s},\mathbf{r}_\mathrm{g}} \int \mathrm{d}\omega\ \omega^2\ \mathrm{G}_0(\mathbf{r}, \mathbf{r}_\mathrm{s}, \omega) \times \left[G_0(\mathbf{r}_\mathrm{g}, \mathbf{r}, \omega)\delta\mathrm{P}^*(\mathbf{r}_\mathrm{g}, \mathbf{r}, \omega)\right],$$

Where $G_0(\mathbf{r}, \mathbf{r}_\mathrm{s}, \omega)$ is the source wavefield and $G_0(\mathbf{r}_\mathrm{g}, \mathbf{r}, \omega)$ is the receiver wavefield. However, since we are interested in updating the background/transmission part of the velocity model, we find the derivative of the misft function with respect to the background part of the velocity model to obtain

$$g(\mathbf{r}) = \sum_{\mathbf{r}_s,\mathbf{r}_g} \int d\omega\ \omega^2\ \left(\delta G(\mathbf{r}, \mathbf{r}_\mathrm{s}, \omega) \times \left[G_0(\mathbf{r}_\mathrm{g}, \mathbf{r}, \omega)\delta P^*(\mathbf{r}_\mathrm{s}, \mathbf{r}_\mathrm{g}, \omega)\right] + G_0(\mathbf{r}, \mathbf{r}_\mathrm{s}, \omega) \times \left[\delta\mathrm{G}(\mathbf{r}_\mathrm{g}, \mathbf{r}, \omega)\delta P^*(\mathbf{r}_\mathrm{s}, \mathbf{r}_\mathrm{g}, \omega)\right]\right),$$

Where $\delta G(\mathbf{r}, \mathbf{r}_\mathrm{s}, \omega)$ is the demigrated source wavefield, $G_0(\mathbf{r}, \mathbf{r}_\mathrm{s}, \omega)$ is the source wavefield, $G_0(\mathbf{r}_\mathrm{g}, \mathbf{r}, \omega)$ is the receiver wavefield, and $\delta G(\mathbf{r}_\mathrm{g}, \mathbf{r}, \omega)$ is the demigrated receiver wavefield.

Examples

To examine RWI, we adopt Wang et al. (2013) model, where we use a three-layer model of dimension 5000 m x 3000 m (Figure 2a). The model is composed of a background velocity of 2500 m/s with a low-velocity Gaussian anomaly, where the center of the lens has a velocity of 2200 m/s. The first reflector is at 3000 m in depth, with a velocity of 2750 m/s. The second reflector has a velocity of 3000 m/s, with a dipping angle. Fifty shots were used in this test, with the first shot at x = 75 m, the last shot at x = 7425 m, and a shot spacing of 150 m. There are 499 receivers in this test, with the first receiver at x = 5 m, the last receiver at x = 7500 m, with receiver spacing of 5 m. The recording time is 3.5 s and the time interval is 3.0 ms. A Ricker wavelet with 10 Hz dominant frequency is used to generate the data. A constant velocity model is used as an initial model with a velocity of 2500 m/s (Figure 2b). RWI is formulated such that the

observed data consists of only reflected waves; hence, we mute direct waves in our observed data. We copare RWI results with FWI results for the same model; however, in FWI we utilize the full recorded information.

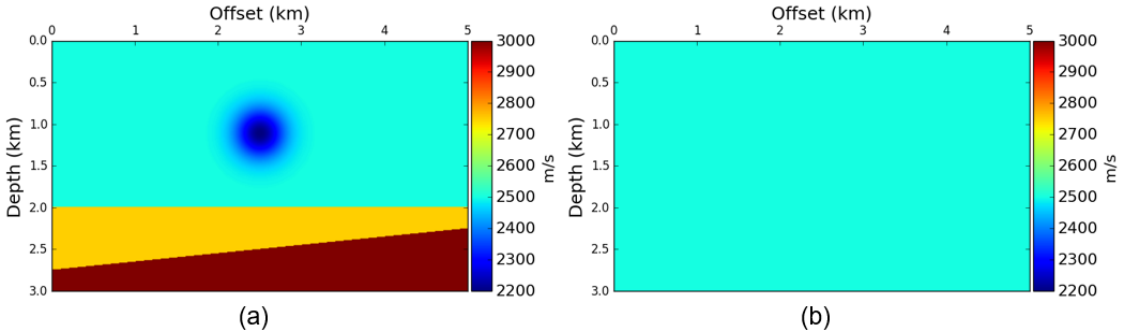

Figure 2: (a) True velocity model. (b) Initial velocity model.

Figures 3a and 3b shows the conventional FWI gradient and the updated model, respectively, after one iteration. As expected, conventional FWI recovered the reflectivity model, but not the Gaussian anomaly that contributes to the background model. FWI failed in retrieving the low-wavenumber components of the velocity model due to the lack of low-frequency information in the data. As a consequence, the reflectivity model below the Gaussian anomaly is unfocused and mispositioned.

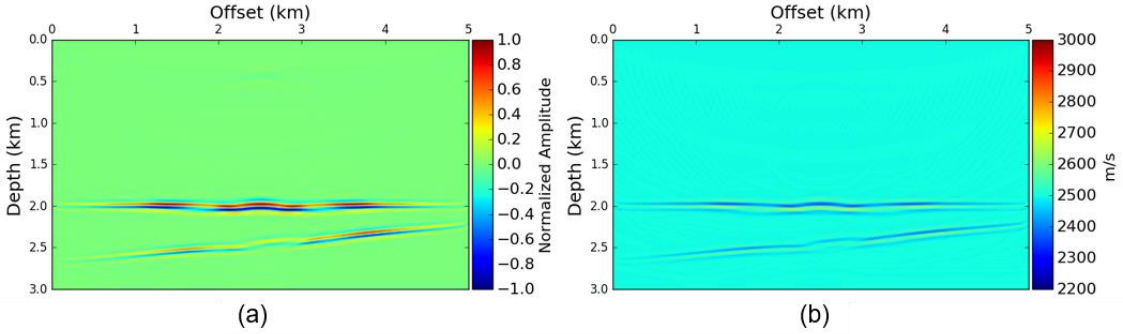

Figure 3: (a) FWI gradient. (b) Updated velocity model using FWI after one iteration.

Figures 4a and 4b shows the RWI gradient and the inverted velocity model after one iteration, respectively. We note that, unlike FWI, RWI recovered the general characteristics of the background model, and the misplaced reflectors in FWI are now correctly positioned.

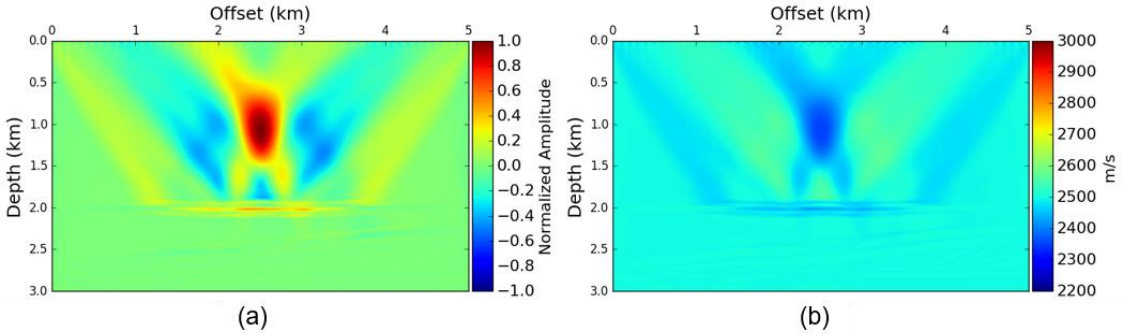

Figure 4: (a) RWI gradient. (b) Updated velocity model using RWI after one iteration.

Figures 5a, 5b, and 5c are the RTM images produced by using the initial velocity, the FWI inverted velocity, and the RWI inverted velocity, respectively, as the migration velocity. The migrated images using the initial velocity and the FWI velocity are both unfocused due to the inaccuracy of the models. On

the other hand, the migrated image using the RWI inverted velocity shows better results and produces a well-focused image.

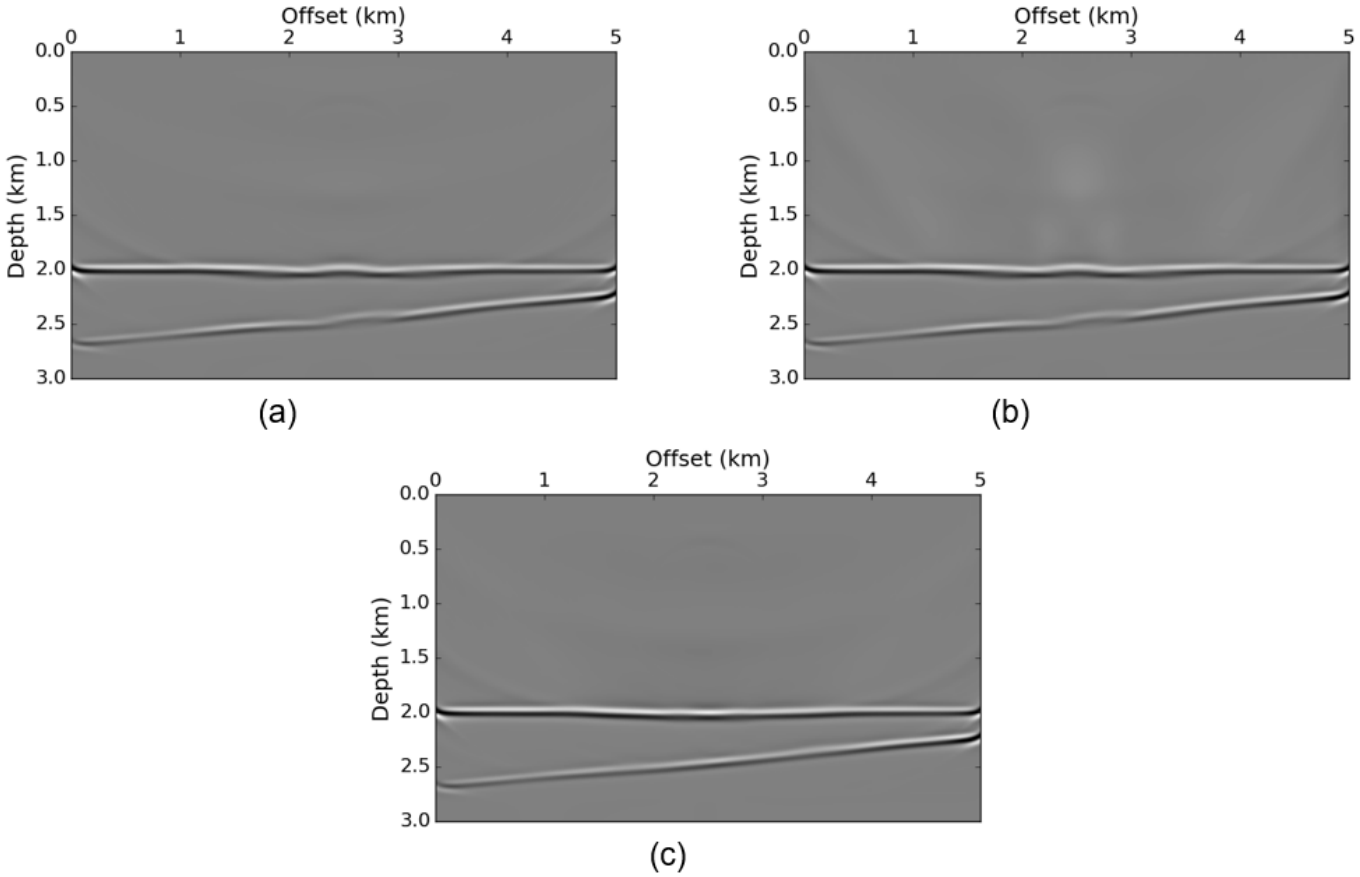

Figure 5: (a) RTM image migrated using the initial velocity. (b) RTM image migrated using the FWI inverted velocity. (c) RTM image migrated using the RWI inverted velocity.

Conclusions

In this paper, we showed that RWI is superior to FWI in retrieving long-wavelength components when building velocity models from reflection data. The background model does not generate backscattering; however, it controls the arrival times of reflected data. As a result, an accurate background model is necessary for seismic migration coherency.

Acknowledgements

We thank the sponsors of CREWES for continued support. This work was funded by CREWES industrial sponsors and NSERC (Natural Science and Engineering Research Council of Canada) through the grant CRDPJ 461179-13. he first author would like to thank Saudi Aramco for graduate study sponsorship.

References

Brossier, R., Operto, S., and Virieux, J., 2015, Velocity model building from seismic reflection data by full-waveform inversion: Geophysical Prospecting, 63, No. 2, 354–367.

Chi, B., Dong, L., and Liu, Y., 2015, Correlation-based reflection full-waveform inversion: Geophysics, 80, No. 4, R189–R202.

Devaney, A. J., 1982, A filtered backpropagation algorithm for diffraction tomography: Ultrasonic imaging, 4, No. 4, 336–350.

Lailly, P., 1983, The seismic inverse problem as a sequence of before stack migrations, in Conference on Inverse Scattering: Theory and Application, Society of Industrial and Applied Mathematics, 206–220.

Miller, D., Oristaglio, M., and Beylkin, G., 1987, A new slant on seismic imaging: Migration and integral geometry: Geophysics, 52, No. 7, 943–964.

Pan, W., and Innanen, K., 2015, Full-waveform inversion in the frequency-ray parameter domain: CREWES Annual Report, 27.

Tarantola, A., 1984, Inversion of seismic reflection data in the acoustic approximation: Geophysics, 49, No. 8, 1259–1266.

Virieux, J., and Operto, S., 2009, An overview of full-waveform inversion in exploration geophysics: Geophysics, 74, No. 6, WCC127–WCC152.

Wu, R.-S., and Toksöz, M. N., 1987, Diffraction tomography and multisource holography applied to seismic imaging: Geophysics, 52, No. 1, 11–25.

Xu, S., Wang, D., Chen, F., Zhang, Y., and Lambare, G., 2012, Full waveform inversion for reflected seismic data, in 74th EAGE Conference and Exhibition incorporating EUROPEC 2012.

Zhou, H., Amundsen, L., and Zhang, G., 2012, Fundamental issues in full waveform inversion, in SEG Technical Program Expanded Abstracts 2012.